ACS APPLIED MATERIALS & INTERFACES

www.acsami.org

Research Article

Superhydrophobic and Recyclable Cellulose-Fiber-Based Composites for High-Efficiency Passive Radiative Cooling

Yanpei Tian,[⊥] Hong Shao,[⊥] Xiaojie Liu, Fangqi Chen, Yongsheng Li, Changyu Tang,* and Yi Zheng*

Cite This: https://doi.org/10.1021/acsami.1c04046

Read Online

ACCESS | Metrics & More | Article Recommendations | Supporting Information

ABSTRACT: Passive daytime radiative cooling (PDRC) involves cooling down an object by simultaneously reflecting sunlight and thermally radiating heat to the cold outer space through the Earth's atmospheric window. However, for practical applications, current PDRC materials are facing unprecedented challenges such as complicated and expensive fabrication approaches and performance degradation arising from surface contamination. Herein, we develop scalable cellulose-fiber-based composites with excellent self-cleaning and self-cooling capabilities, through air-spraying ethanolic poly(tetrafluoroethylene) (PTFE) microparticle suspensions embedded partially within the microsized pores of the cellulose fiber to form a dual-layered structure with PTFE particles atop the paper. The formed superhydrophobic PTFE coating not only protects the cellulose-fiber-based paper from water wetting and dust contamination for real-life applications but also reinforces its solar reflectivity by sunlight backscattering. It results in a subambient cooling performance of 5 °C under a solar irradiance of 834 W/m^2 and a radiative cooling power of 104 W/m^2 under a solar intensity of 671 W/m^2. The self-cleaning surface of composites maintains their good cooling performance for outdoor applications, and the recyclability of the composites extends their life span after one life cycle. Additionally, dyed cellulose-fiber-based paper can absorb appropriate visible wavelengths to display specific colors and effectively reflect near-infrared lights to reduce solar heating, which synchronously achieves effective radiative cooling and esthetic varieties.

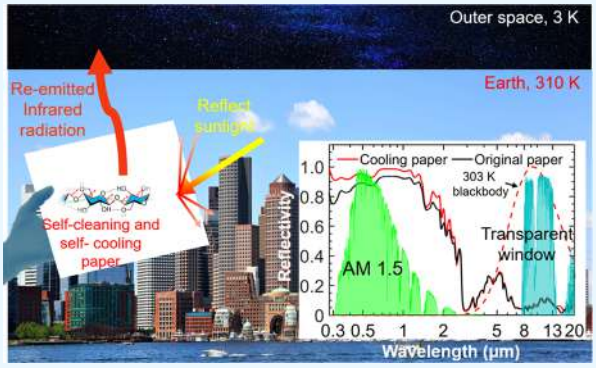

KEYWORDS: *passive daytime radiative cooling, cellulose fiber, superhydrophobic, self-cleaning, scalable-manufactured, recyclable*

INTRODUCTION

Compressor-based cooling systems, providing comfortable interior environments for artificial structures (e.g., buildings), account for about 20% of the total electricity consumption around the world in 2019.[1] Moreover, the resultant heating effects[2] and greenhouse gas emissions toward the environment[3] accelerate global warming and climate changes. Therefore, energy-efficient and eco-friendly cooling approaches are highly demanded for energy-saving techniques. The emerging passive daytime radiative cooling (PDRC) technique can achieve subambient cooling effects under direct sunlight without any energy consumption by simultaneously reflecting sunlight (0.3−2.5 μm) and radiating excessive heat as infrared thermal radiation to the cold outer space through the atmospheric transparent window (8−13 μm).[4−6] A typical PDRC structure should have both high solar reflectivity (R_{solar}) and high infrared thermal emissivity (ϵ_{IR}) so that a net radiative heat loss can be achieved even under sunlight.[7] Such an approach is becoming an attractive candidate for improving energy efficiencies for buildings because it eliminates the need for coolant, electricity, and compressor required by traditional mechanical cooling systems.

PDRC structures with high R_{solar} and high ϵ_{IR} have been widely investigated in recent decades including photonic structures,[4,8−10] metallized polymers,[11−13] white paints,[14−16] and dielectric−polymer hybrid metamaterials.[5,7,17,18] Design and fabrication of these subambient cooling structures are either complicated or costly. Even worse, they are susceptible to contamination by floating dust, dirt, and soot when exposed to the outdoor environment.[19] As a result, surface contamination deteriorates the solar reflectivity since the color of the dust that is mostly gray may severely absorb the solar energy in the visible regions. More absorbed solar energy enhances the solar heating effect on the PDRC structures and therefore deteriorates their self-cooling performance (Figure S1). For practical applications, PDRC structures often need frequent cleaning, which is time- and labor-intensive, to maintain their unique optical properties. These issues have hindered PDRC

Received: March 5, 2021
Accepted: April 23, 2021

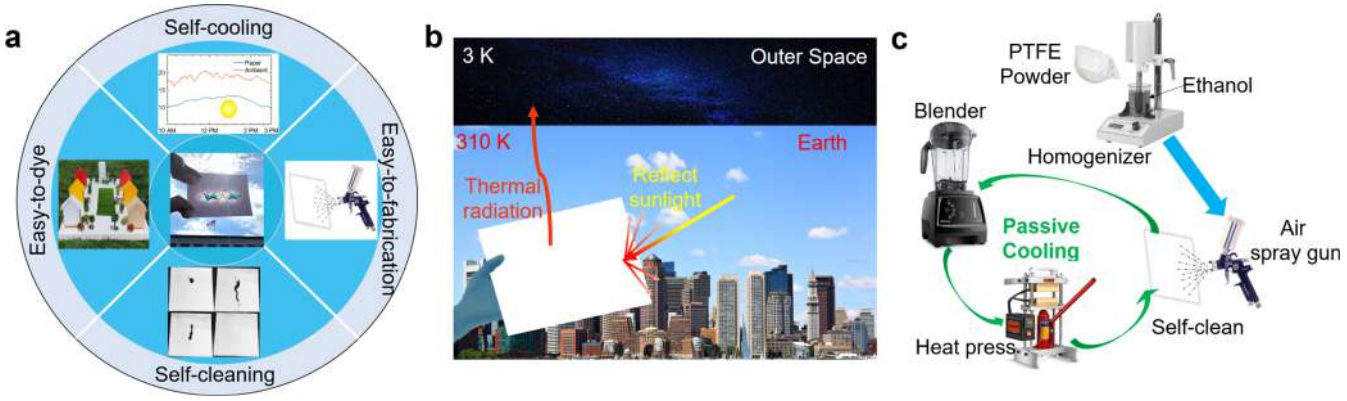

Figure 1. (a) Multifunctional paper-based composites with self-cooling and self-cleaning properties can be easily fabricated and dyed. (b) Photograph and schematic showing that the composites strongly backscatter the solar irradiance and re-emit thermal radiation, resulting in a net radiative heat loss to the outer space. (c) Fabrication and recycle processes of the cooling paper.

structures for real-life applications. The micro/nanostructures of photonic metamaterials are on the same scale as the dust floating in the air, and this makes the contamination possible, which will severely decrease both their solar reflectivity and thermal emissivity. The wetting ability of the metalized polymers, white paints, and dielectric−polymer hybrid metamaterials reported before is either missing or unsatisfactory. To the best of our knowledge, the investigation of cooling structures with stable self-cleaning ability has been rarely reported. Furthermore, colored buildings are always desirable for esthetic purposes,[20,21] so white or silvery surfaces, based on the wide-band reflectivity in visible wavelengths, confine their wide applications for infrastructures.

The cellulose-fiber-based paper that is widely used in our daily life has emerged as a low-cost engineering material for various devices (e.g., electronic device and paper-based lab on a chip) due to its earth abundance, biodegradability, and remarkable optical and mechanical properties.[22,23] The paper consisting of cellulose fibers (20−50 μm in diameter) can strongly scatter sunlight with a high R_{solar} of about 0.89 and, meanwhile, exhibit an excellent ϵ_{IR} of 0.92 owing to the molecular vibrations of C−O−C and C−O bonds in cellulose.[24] Thus, the paper could be a good candidate for PDRC structures. Delignified wood mostly consisting of cellulose is reported for daytime radiative cooling. Cellulose-fiber-based papers have rarely been investigated for radiative cooling, especially for self-cleaning paper for the outdoor radiative cooling applications. However, the paper is not waterproof and is easily contaminated by dust, resulting in a significant reduction of its optical properties and cooling performance. Herein, we report a simple and scalable method to transform the paper into a self-cooling material with self-cleaning ability. Poly(tetrafluoroethylene) (PTFE) particles, an ultra-white material with extremely high reflectivity (0.3−2.5 μm)[7] and extremely low surface energy, are sprayed into the microsized pores of the cellulose-fiber-based paper by physical adsorption and mechanical locking to form a white superhydrophobic coating with a thickness of ∼30 μm. The water droplets can roll off its surface and take away the dust on the surface presenting good self-cleaning ability. The presence of PTFE coating not only protects the paper from water wetting and dust contamination for outdoor applications but also reinforces its solar reflectivity (R_{solar} = 0.93). Consequently, the PTFE-coated cellulose-fiber-based composites exhibit a sub-ambient cooling of ∼5 °C under a solar irradiance of 834 W/m^2 and a radiative cooling power of 104 W/m^2 under a solar intensity of 671 W/m^2. Their performance is better than or on par with other radiative cooling performances as listed in Table S1. This method can integrate self-cleaning and self-cooling surfaces to various substrates such as brick, metal, wood, and concrete for versatile applications. The superhydrophobic feature ensures that its life cycle is maintenance-free and extends its life span. Besides, the recyclability of the cellulose-fiber-based composites after one life cycle also contributes to their green and energy-saving functionality. Furthermore, the composites have diverse dyeing options to attain the necessity of esthetics along with the modest cooling performance. These advantages (Figure 1a) of the functional self-cooling composites will shed light on an alternative novel cellulose-fiber-based radiative cooling material and provide a promising pathway for green-energy applications.

EXPERIMENTAL METHODS

Materials. The 100 lb paper was provided by International Paper. The spray adhesive was obtained from Gorilla. The PTFE film was purchased from CS Hyde Company. The black dye was obtained from AmeriColor Corporation. Red and yellow dyes were obtained from Rite LLC. All reagents were used as received without further purification. Black 3.0 paint was purchased from the Culture Hustle. Coleman cooler box was purchased on Amazon.

Methods. *Fabrication of White Paper Composites.* Poly(tetrafluoroethylene) (PTFE) microparticles (3 g, 1.4 μm average size in diameter, Sigma-Aldrich) were added into 30 g of ethanol (95% denatured, Innovating Science) and homogenized by a high-speed emulsifier (MXBAOHENG, FSH-2A) at 22 000 rpm for 3 min. The resultant suspension was sprayed on a 12 cm × 13 cm paper using an airbrush equipment (nozzle diameter 0.8 mm) at an air pressure of around 70 psi with a distance of about 10 cm. The mass density of the PTFE coating on the paper was around 2 mg/cm^2. The sprayed paper was dried at 100 °C for 30 min.

Fabrication of Colored Paper Composites. The dye (5 g, Rite LLC) was dissolved into 10 g of DI water and was subsequently sprayed onto a 12 cm × 13 cm paper with the same airbrush using the same parameters with the fabrication of the white paper composites. The paper can also be dyed by dipping it into the dye suspension. The sprayed or dip-coated paper was then dried at 60 °C for 30 min.

Fabrication of the Solid Cellulose Film. Dried cellulose powders (2 g) were placed into a dry pellet pressing die with an inner diameter of 13 mm, and it was pressed at a pressure of 60 MPa for 45 s to form a uniform solid film.

Fabrication of the Black 3.0 Painted Paper. Black 3.0 paint was diluted with DI water under mechanical stirring for 5 min to get a homogeneous mixture. The mass ratio of DI water to Black 3.0 paint

https://doi.org/10.1021/acsami.1c04046
ACS Appl. Mater. Interfaces XXXX, XXX, XXX−XXX

was ~0.4 in the dilution process. Subsequently, the diluted Black 3.0 paint was sprayed onto the paper sheet with a thickness of 0.35 μm using a spray gun (Paasche Airbrush) with a 0.8 mm spray head at a pressure of 70 psi. The distance between the spray head and the paper sheet was about 25 cm. The sprayed paper was dried using a hot blower (Yihua Electronic Equipment Co., Ltd., Guangzhou, China) after each spray at a temperature of 190 °C for 5 min.

Fabrication of the Colored Wood. The red and yellow dyes were thinned with DI water and the mass ratio of dye to water was 1:2. Then, the thinned dye was sprayed on a 2 mm thick basswood sheet using a spray gun with a 0.8 mm spray head at a pressure of 70 psi. The distance between the spray head and the wood sheet was about 10 cm. The sprayed wood sheet was left in the air for 6 h to dry before the dyed wood fabrication.

Recycling Process of Paper Composites. The paper composites were cut into small pieces and immersed in water for 1 h. After that, the swelled paper was smashed into paper pulp using a high-speed blender for 3 min (Vitamix E310). The paper pulp was thermally pressed into a paper sheet by a hydraulic press machine (DABPRESS, 10 Ton) under 20 MPa and 200 °C until the paper was dry. The regenerated paper can be reused for fabricating self-cooling and self-cleaning paper composites by recoating the PTFE particles.

Material Characterization. *Morphology Characterization.* The surface morphologies of samples were examined using a scanning electron microscope (SEM, S5200, Hitachi Company) under an acceleration voltage of 10 kV. The morphology of the pencil-scratched samples was observed using a trinocular metallurgical microscope (ME300TZA-3M) with a 50× lens.

Surface-Wetting Characterization. The water contact angle (CA) of the sample was measured using a contact angle goniometer (DSA-25, Krüss, Germany) with a 7 μL DI water droplet at room temperature according to the sessile droplet method. The reported static contact angles were calculated by averaging the measured values from both the left and right sides of the droplet. Six data points were collected at six different positions on the sample surface and were used for calculating the final average values.

Paper Composition Characterization. The paper composite sample (1 g, ±0.0001 g) was dried at 100 °C for 30 min and was weighed to calculate the moisture content. The PTFE content was identified by measuring the mass change of the paper before and after spraying PTFE. Ethanol (400 mL; 95%) was mixed with 100 mL of HNO_3 for etching other components of the paper to obtain the cellulose. The paper composite sample (1 g, ±0.0001 g) was mixed with 25 g of ethanol−HNO_3 solution in a 250 mL conical flask with a condenser and was subsequently refluxed for 1 h at 100 °C. These procedures were repeated 2−3 times until the paper fibers were white. The above fibers were washed using ethanol until the pH of the filtrate was near 7. Finally, these fibers were dried at 105 °C (± 2 °C) and were weighted for calculating the cellulose content.

Optical Characterization. The reflectivity spectra (0.3−2.5 μm) were measured using a Jasco V770 spectrophotometer at an incident angle of 6° with the ISN-923 60 mm $BaSO_4$-based integrating sphere equipped with PMT and PbS detectors. The reflectivity spectra were normalized by a PTFE-based reflectance standard. The reflectivity spectra (2.5−20 μm) were measured using a Jasco FTIR 6600 at an incident angle of 12° with the PIKE upward gold integrating sphere equipped with a wide-band MCT detector. Angular-dependent reflectivity spectra were measured using wedges with different angles at the sample port of these two integrating spheres, and the measurement mechanism of using the wedges can be found in our previous work.[25] The single-valued R_{solar} and ϵ_{IR} are calculated by integrating the reflectivity spectra or emissivity spectra based on the AM 1.5 or 303 K blackbody spectra, respectively.

Refractive Index Characterization. The complex refractive index of the sample was measured using an ellipsometer (J.A. Woollam, M-2000DI) with an incident angle of 60−70° and a spectral range of 0.38−0.9 μm.

Size Distribution Characterization. The size distribution of the cellulose fibers and PTFE particles was determined by ImageJ software according to the SEM images, in which 200 points were randomly selected for each image.

Finite-Difference Time-Domain (FDTD) Simulation. FDTD simulation was executed using Lumerical FDTD Solution 2018a. Two-dimensional models were employed, and a total-field scattered-field source coupled with two scattering cross sections of cellulose fibers and PTFE particles was used to calculate the scattering efficiency. The cross section of the paper fibers is 28 μm × 28 μm, and the cross section of the PTFE particles is a circle with a diameter of 1.4 μm. Different shapes of cross sections were also simulated to check the effects of various shapes on the scattering efficiency.

Scattering Effects Measurement. One layer of paper fibers was peeled off from the original paper using the Tape King packaging tape. PTFE particles (0.2 g) were uniformly smeared on the adhesive side of the packing tape (CS Hyde company). These cellulose fibers and PTFE particles were placed at the aperture position, which is between the laser pens (red, green, and purple) and the blackboard. The area of scattered laser spots was used to indicate the scattering effect of paper fibers and PTFE particles.

Infrared Image Measurement. Infrared images were taken using an FLIR A655C thermal camera with a 25° lens at a resolution of 640 × 480.

Cooling Power and Temperature Tracking. All of the materials were placed inside a 100-Quart modified cooler box (excellent thermal insulation) with the removal of the top lid. For the cooling power measurement chamber, the top surface of the paper composites (12 cm × 13 cm × 2 mm) faces the clear sky through a 20 μm thick HDPE film. The air gap between the paper composites and the HDPE film was around 5 mm. The paper composites were glued to the supporting copper sheet below (12 cm × 13 cm × 0.9 mm, thermal conductivity, TC, 380 W/(m·K)) using a silver thermal compound paste (TC, 8.5 W/(m·K)). The Kapton thin-film heater (11 cm × 11 cm × 0.4 mm) was glued to the supporting copper sheet with the same silver thermal paste, and the temperature of the paper composites sample was measured using the K-type thermocouples connected to the National Instruments (NI) PXI-6289 multifunction I/O module. The "ON" and "OFF" of the heater were controlled by the NI PXI-2586 relay module driven by a home-built LabVIEW program using the PID control algorithm to maintain the temperature of the paper composites by tracking the ambient air. The K-type thermocouples were welded to the copper sheet using epoxy resin. The 6 mm thick aerogel blankets used here have a thermal conductivity of ~23 mW/(m·K) to reduce the heat transfer between the PVC insulation foam and samples. The PVC insulation wall has a thickness of 25 mm with thermal conductivity of ~31 mW/(m·K).

Thermal Conductivity Measurement. The thermal conductivity of the one-layer paper was characterized by the TPS 2500s thin-film module, while the thermal conductivities of the basswood and concrete were measured by the isotropic standard module of TPS 2500s.

Mechanical Strength Measurement. The mechanical strengths of the paper sheet (2 cm × 6 cm × 0.35 mm) and a basswood slab (2 cm × 6 cm × 1.5 mm) were measured using a Mark-10 ESM tensile tester at room temperature.

Validation of the Self-Cleaning for Paper Composites. The original paper and the self-cleaning paper composites with a dimension of 10 cm × 8 cm × 0.35 mm were placed on a wedge with an oblique angle of 10°. One drop of black dye (0.12g) and 0.31 g of garden soil were stained on the original paper and the self-cleaning paper. Then, water from the squeeze bottles washed the black dye and the garden soil, and the wash process was recorded in a phone camera.

Abrasion Robustness Tests. A sandpaper abrasion test was carried out using a 400 grit SiC sandpaper as an abrasion surface. The sample was fixed to a glass slide with a loaded weight of 50 g and placed face down onto the sandpaper, and then moved 10 cm along the ruler. Subsequently, the sample was rotated by 90° and again moved 10 cm along the ruler.[26] The two aforementioned steps are defined as one abrasion cycle. This process guarantees that the paper composite surface is abraded longitudinally and transversely in each cycle.

https://doi.org/10.1021/acsami.1c04046
ACS Appl. Mater. Interfaces XXXX, XXX, XXX−XXX

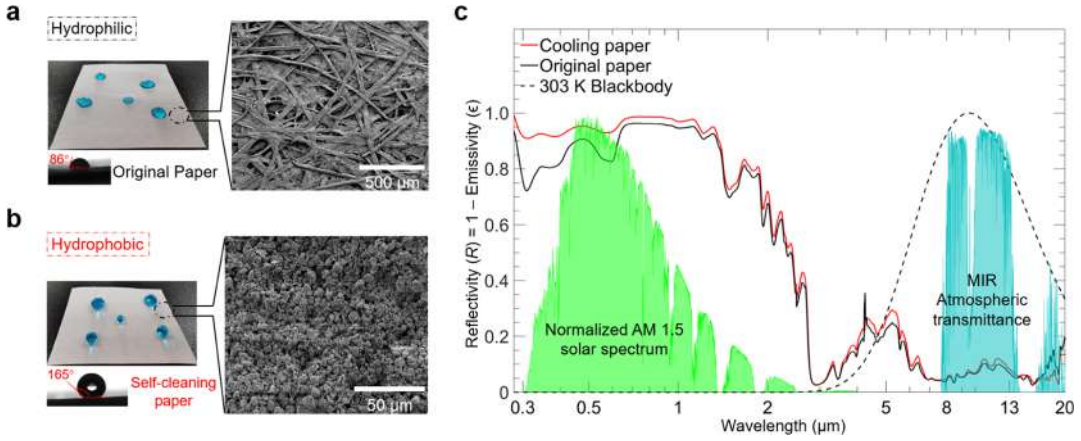

Figure 2. Surface-wetting states and microstructures of (a) the original paper and (b) PTFE-coated paper composites (cooling paper). (c) Hemispherical spectral reflectivity ($R = 1 - \epsilon$) of the original and composites displayed with the normalized ASTM G-173 (AM 1.5) solar spectrum, the mid-infrared (MIR) atmospheric transparent window (MODTRAN 4), and the spectral irradiation of a 303 K blackbody.

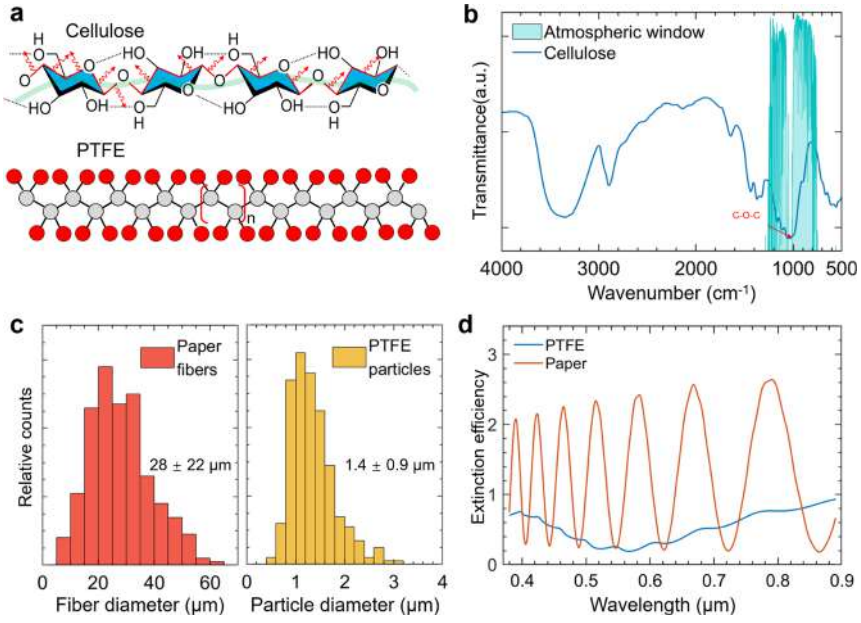

Figure 3. (a) Schematic showing the molecular structures of cellulose and PTFE (the main components of the composites) and the thermal emissions (red arrows) from the molecular vibrations of C−O−C bands in the MIR region. (b) FTIR transmittance spectrum of the cellulose presenting C−O−C absorption bands located at the atmospheric transparent window. (c) Size distributions of the cellulose-fiber-based paper fibers and PTFE particles. (d) FDTD-simulated scattering cross section spectra of the cellulose fibers and PTFE particles that show a high scattering efficiency over solar wavelengths, resulting in a high R_{solar}.

Antiscratch Tests. A set of pencils with different hardness (10B-9B-8B-7B-6B-5B-4B-3B-2B-B-F-HB-H-2H-3H-4H-5H-6H-7H-8H-9H) were selected to make a scratch on the paper composite surface. The pencil was held at 45° to the paper composites and pushed for a scratch length of 10.0 mm. The micrographs of the paper after scratch tests were used to analyze its antiscratch property.

Raindrop Tests. The simulated raindrop tests were conducted using a syringe pump at a flow rate of 3 mL/h from a 17 gauge syringe needle for 7 days. The needle head was about 35 cm over the paper composites. The oblique angle of the paper composites was fixed at 10°.

Peel-off tests. An XFasten tape (6 cm × 2 cm) was pressed onto the paper composites and was peeled off at a speed of about 1 cm/s.

Harsh Environment Exposure. To test the long-term durability of the paper composites under different harsh environment exposures, the paper composites were placed in a freezer (−20 °C), an incubator (60 °C, RH ≈ 100%), a convection oven (80 °C, RH ≈ 0%), and a UV lamp (UV density, 3 mW/cm^2) for 30 days, respectively.

RESULTS AND DISCUSSION

The original paper consists of random-stacked cellulose fibers with porous structures (Figures S1 and S2). The paper composites are fabricated by air-spraying the homogeneous PTFE microparticle suspension (3 g/30 g, PTFE/ethanol) onto the original paper followed by solvent evaporation to form a self-cleaning and self-cooling surface (Figures 1a−c, S3, and S4). The PTFE microparticles with an average size of 1.4 μm are embedded into the microsized pores (20 μm) of the cellulose-fiber-based paper formed by the stacked cellulose fibers and form a white coating. The random-stacked fibers with PTFE particles efficiently scatter sunlight from ultraviolet to near-infrared wavelengths and throw heat into the cold outer space (Figure 1b). The easy recyclability of the self-cooling paper extends its life span after one life cycle (Figure 1c). Meanwhile, the PTFE particles form a rough surface with

https://doi.org/10.1021/acsami.1c04046
ACS Appl. Mater. Interfaces XXXX, XXX, XXX−XXX

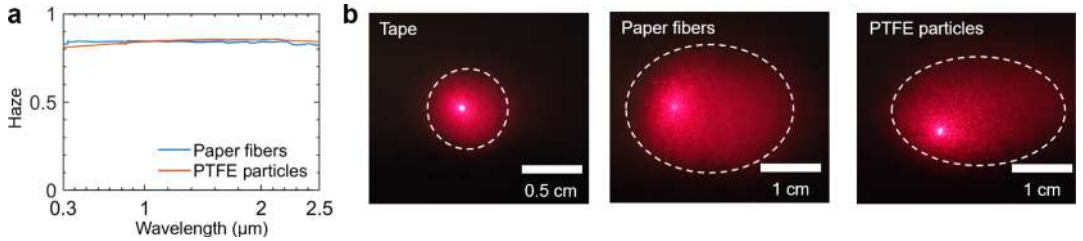

Figure 4. (a) Transmission haze spectra of the paper fibers and PTFE particles with an incident angle of 0°. (b) Laser images showing the scattering effects of a red laser shining at the cellulose fibers and PTFE particles sticking on a tape film. The clear tape is a biaxially oriented polypropylene film, which hardly scatters the red laser beam.

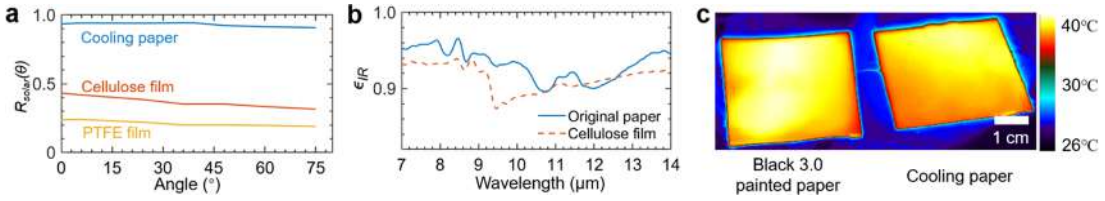

Figure 5. (a) Solar reflectivity (R_{solar}) of the paper composites for different incident angles from 0 to 75° compared with the solid cellulose and PTFE films with the same thickness (700 μm). (b) Infrared emissivity (ϵ_{IR}) of the original paper and the cellulose film from 7 to 14 μm. (c) Infrared images of a Black 3.0 (infrared-ultrablack materials) painted paper and composites sitting on top of a hot plate. The paper composites show high ϵ_{IR} similar to the Black 3.0 painted paper. The deep blue area is the aluminum foil that has little thermal emission in the MIR region.

micro/nanostructures, which transform the paper from a hydrophilic (contact angle, θ = 86°) to a superhydrophobic state (θ = 165°) (Figures 2a,b, S4 and Video S1). This feature enables the waterproof and self-cleaning surface of the composites for outdoor applications. Interestingly, R_{solar} of the cellulose-fiber-based paper is enhanced from 0.89 to 0.93 after PTFE coating, compared with the original paper. This result could be attributed to the PTFE microparticle coating that reinforces the sunlight scattering of the paper (Figures 2c and S2). The high hemispherical solar reflectivity (nearly "white") and infrared emissivity (nearly "black") of the composites ensure that it radiates a net heat flux to the cold outer space sink as infrared thermal radiation (Figure 2c). The heat radiated by the composites exceeds the heat gained from the solar absorption and the atmosphere, thus leading to subambient cooling effects. In the outdoor environment, sunlight irradiates the Earth with different incident angles all day and is partly polarized by the dust in the air. These factors can affect the optical response of PDRC structures, which is generally undesirable. Fortunately, both solar reflectivity and thermal emissivity of the paper composites are angle-independent even at a large angle of incidence (AOI, θ = 75°) (Figure S5), which is attributed to the porous and rough surface. The randomly arranged cellulose fibers and PTFE particles give rise to a polarization-independent R_{solar} and ϵ_{IR} (Figure S5). With these unique structures, the cellulose-fiber-based composites show the diffused white and black features from 6 to 75° in the solar wavelengths and atmospheric transmittance window, respectively, yielding high R_{solar} and ϵ_{IR} (greater than 0.9, Figure S5) when the paper composites face toward different angles of the sky in real-life applications.

Radiative Cooling Mechanism of Paper Composites. Cellulose and PTFE (Figure 3a) are two major components of the paper composites, and they own intrinsic optical properties for the PDRC applications. The Fourier transform infrared (FTIR) transmission spectra show that cellulose, lignin, and PTFE in the paper composites exhibit strong emission bands at 800−1200 and 1040 cm^{-1}, which are assigned to the vibrations of C−O−C of cellulose, vibrations of syringyl and guaiacyl rings of lignin, and asymmetric and symmetric stretching bands of CF_2 of the PTFE (Figures 3b and S6).[27−29] This result implies that the infrared emission bands of the composites coincidentally fall in the atmospheric transparent window. The negligible extinction coefficient of the cellulose and PTFE from 0.38 to 0.9 μm (covering half wavelength range of the solar irradiance) makes the paper composites an ideal reflector of the solar irradiance (Figure S7). The innate structure of the paper composites with PTFE microparticles and cluttered cellulose fibers presents high R_{solar} and ϵ_{IR}. The diameter of cellulose fibers ranges from 6 to 50 μm centering at 28 μm, while the PTFE particles span within 1.4 ± 0.9 μm (Figure 3c). The cellulose microfibers efficiently backscatter the sunlight, which is further enhanced by adding submicron PTFE particles, as shown by the scattering cross section efficiency spectra simulated using the finite-difference time-domain (FDTD) methods (Figures 3d and S7). The cellulose-fiber-based paper has both large and small fibers. The large fibers act as the skeleton of the paper and give rise to a good mechanical strength, and the small fibers interconnect those large fibers as an adhesive to enhance the mechanical strength further. The small fibers also reduce the surface roughness of the paper to increase its solar reflectivity. The pores among the cellulose fibers can trap and fix PTFE particles for producing self-cleaning functionality. The transmission haze spectra of the paper and PTFE particles show that the self-cooling paper has a high haze value of about 0.8 on average (Figure 4a). The scattering effects of the cellulose fibers and PTFE particles are visualized using a red laser beam with a wavelength of 650 nm traveling through the cellulose fibers and PTFE particles sticking on a clear tape film (Figure 4b). The illuminated area is much larger than that of the one of the clear tape films indicating strong scattering effects from the paper fibers and particles; similar phenomena are observed for the green and violet laser beams (Figure S8). The disordered cellulose fibers and PTFE particles result in a diffused white surface compared to the solid cellulose and PTFE films (Figures 5a and S9) with

https://doi.org/10.1021/acsami.1c04046
ACS Appl. Mater. Interfaces XXXX, XXX, XXX−XXX

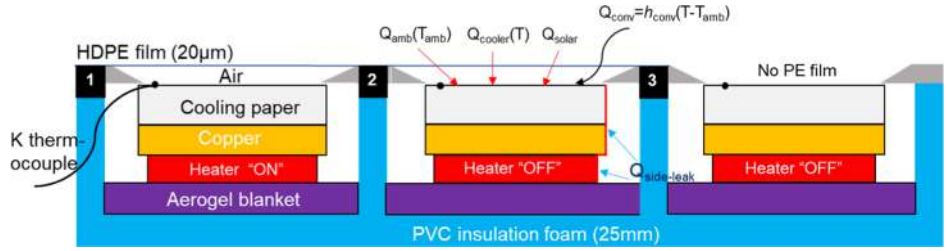

Figure 6. Schematic of the setup in chamber a-1 for the real-time measurement of subambient cooling performance under sunlight. Chamber a-2: The same setup as a-1 but without the PID temperature tracking system; the heater here stays "OFF". Chamber a-3: the same setup as a-2 without the HDPE film covered, i.e., the hierarchical paper composites are open to air without the PE shield (T_i refers to the surface temperature of sample a-i).

an AOI from 0 to 75°. The paper composites have a higher infrared emissivity than the cellulose film, which is attributed to their components (cellulose, hemicellulose, and lignin) and the random-cluttered cellulose fibers (Figures 2a,b, 5b, S1, and S2). The high ϵ_{IR} of the paper composites is comparable to that of an infrared-ultrablack paint (black 3.0, $\epsilon_{IR} \approx 0.99$), which is validated by the infrared images and reflectivity spectra as shown in Figures 5c and S10.

Outdoor Validation of the Paper Composites Cooling Performance. The subambient cooling performance of the paper composites during a one-day cycle has been demonstrated on a rooftop at Northeastern University, Boston, MA. A six-layer paper (opaque to the sunlight, Figures S11 and S12) is glued layer by layer as the test sample with the top layer sprayed with PTFE microparticles (Figure 6 and Table S2). The temperature tracking curve shown in Figure S11 indicates that the top surface temperature of the composites follows the ambient temperature with a bias of ±0.2 °C (Figure S13), indicating a reliable measurement accuracy of the radiative cooling performance of the composites. The paper composites have an averaged radiative cooling power of about 75 W/m^2 over a one-day cycle. The average cooling powers of the paper composites are 82.3 and 71.6 W/m^2 at the daytime and night-time, respectively (Figure 7a). This is attributed to the night-time relative humidity (70% RH, averaged, low atmospheric transmittance) being higher than that during the daytime (55.3%, averaged, high atmospheric transmittance) and the night-time wind speed (1.9 km/h, averaged, low air convection) being much lower than that during the daytime (5.4 km/h, averaged, high air convection) (Figure S13). The averaged ΔT_2 (4.4 °C) is higher than the averaged ΔT_3 (2.4 °C) during the night and vice versa during the day (ΔT_2 = 5.1 °C < ΔT_3 = 6.1 °C) (Figure 7b,c). During the night-time, the solar heating effects disappear, and the only heating effect comes from the radiative heat transfer from the ambient air and the nonradiative heating from the heat conduction of the supporting structure for the sample and the wind convection heating. The HDPE cover serves as a wind cover to block convection heating from air. Thus, chamber a-2 with the HDPE cover has a larger temperature drop during the night-time. During the daytime, since the HDPE film is not fully transparent to the mid-infrared wavelengths (averaged transmittance is around 0.9 based on the 303 K blackbody radiation), it will block part of the radiative heat transfer between the self-cooling paper and the cold outer space. At the same time, the HDPE has an average transmissivity of around 0.89 over the solar radiation wavelengths, and it will reflect parts of the solar irradiation to the surface of the self-cooling paper and the air in the small space between the self-cooling

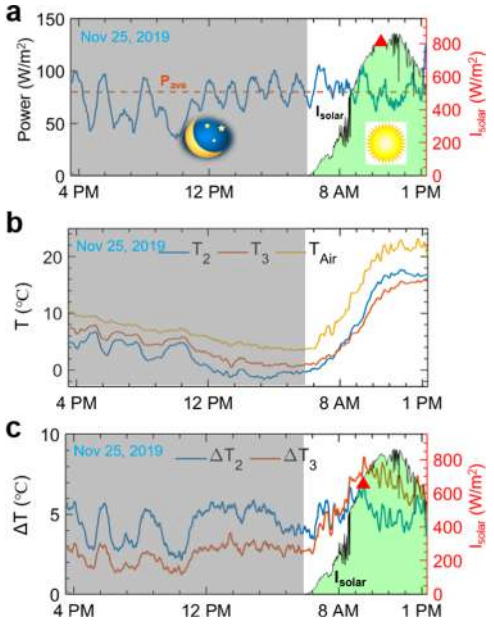

Figure 7. (a) Cooling power of the paper composites in a one-day cycle. (b) Temperature variations of the paper composites in chambers a-2, a-3, and the ambient. (c) Temperature difference between the ambient and the paper composites in a-2 and a-3, respectively.

paper and the HDPE cover. The increasing temperature of the small space will also heat the self-cleaning paper up. The wind temperature is lower than the ambient since the ambient temperature thermocouple is enclosed inside a wind cover similar to the weather station. This method to measure the ambient temperature is also used in meteorology. The wind will bring heat from the self-cooling paper in a-3 immediately. Therefore, the temperature of a-2 is greater than that of a-3 because the HDPE windshield blocks the heating from the air at night resulting in lower temperatures from the radiative cooling effect. However, the cooling effect from the high-speed wind is partially blocked by the HDPE film in a-2 compared with the one in a-3. Consequently, the PTFE-coated cellulose-fiber-based composites exhibit a subambient cooling of ~5 °C under a solar irradiance of 834 W/m^2 and a radiative cooling power of 104 W/m^2 under a solar intensity of 671 W/m^2 (as marked by a red triangle in Figure 7a,c). The various external factors (solar intensity, nonradiative heat transfer, and atmospheric transmittance) are discussed in Figure S14 and the Supporting Notes. Compared with the common building materials such as wood and concrete, the temperature of the composites is 8.1 °C lower than the one made of basswood

https://doi.org/10.1021/acsami.1c04046
ACS Appl. Mater. Interfaces XXXX, XXX, XXX−XXX

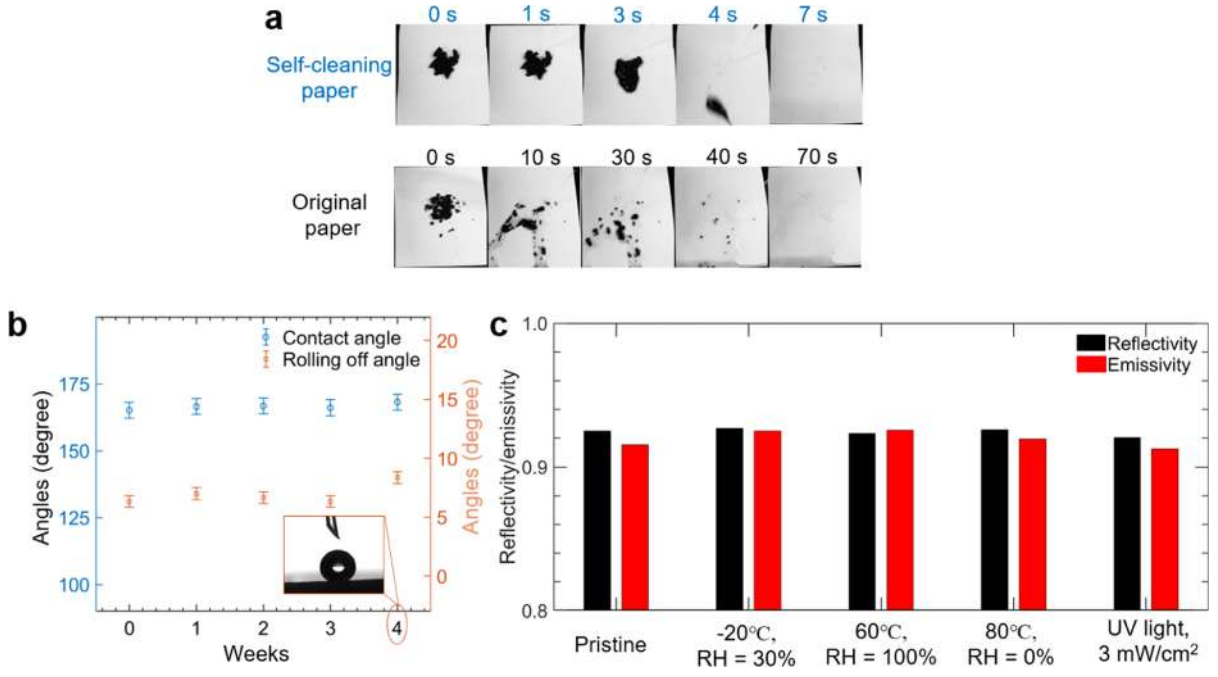

Figure 8. (a) Self-cleaning properties of the paper composites when stained with the garden soil. (b) Contact angle and rolling-off angle of the paper composites after outdoor exposure at different times. Inset shows the water contact angle of paper composites after a four-week outdoor test. (c) Overall solar reflectivity and thermal emissivity of the cooling suffering from various harsh environmental factors for 30 days.

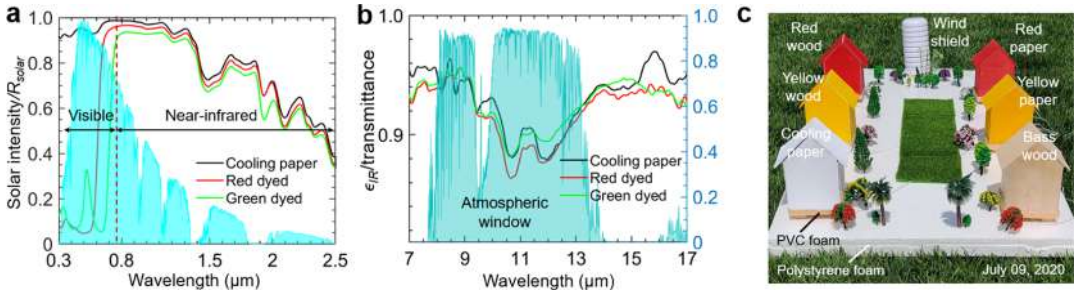

Figure 9. R_{solar} (a) and ϵ_{IR} (b) of the red- and green-dyed papers compared to the paper composites. (c) Photograph of the setup for recording the temperature under sunlight.

(Figures S15–S17), attributing to the self-cooling function and the lower thermal conductivity of the composites than that of the basswood and concrete (Figures S18–S19). As shown in Figure S15, the composites in a-3 without a windshield are 2.8 °C cooler than the ambient and have an averaged 32 W/m^2 cooling power at noontime in the mid-summer (Figure S16).

Surface Stability of Paper Composites. The paper composites are mechanically robust because of hydrogen-bond interactions and friction forces between fibers (Figure S20).[30] This can be easily cemented to common materials like brick, metal, wood, and concrete for outdoor utilization (Figure S21). The composites often suffer from complicated environmental factors such as dust contamination, UV exposure, temperature and humidity change, mechanical abrasions, raindrop washing, and scratches, any of which may degrade their optical properties and cooling performance in an outdoor environment (Figure S1). This issue was usually neglected in previous studies.[5,6,31] We examine the long-term stability of the composites under a simulated environment (Figures 8a–c and S22–S30). Black dye and garden soil are employed to contaminate both the original paper and paper composites. The original paper is easily dyed by black dye and the soil on its surface is not easily washed away, resulting in reduced light reflectivity. In contrast, the paper composites remain clean without any dying and the residual soil because of their excellent self-cleaning ability arising from the superhydrophobic PTFE coating (Figures 8a and S22). The self-cleaning durability of the cellulose-fiber-based composites is demonstrated by a four-week outdoor exposure with little changes observed in the contact angle and the rolling-off angle (Figures 8b and S22–S23). The 15-min water immersion test shows good waterproof properties for outdoor utilization (Figure S24). Additionally, different harsh environmental tests, such as UV exposure, raindrop impact, low and high-temperature exposure, high humidity exposure, and mechanical abrasions, do not lead to any change in the optical performance and self-cleaning property (Figures 8c and S25–S30). This indicates good surface stability of the paper composites, which is a benefit to keeping its good cooling performance for outdoor applications. The PTFE layer of the composites can also reduce the friction of the surface of the composite, avoiding scratches from hard objects (Figure S31). After cyclic peel-off tests, the reflectivity and emissivity of the paper composites show no significant change (both are within 3%), demonstrat-

https://doi.org/10.1021/acsami.1c04046
ACS Appl. Mater. Interfaces XXXX, XXX, XXX–XXX

ing their robust cooling performance (Figure S32). It is also experimentally demonstrated that the recycled composites still yield a self-cooling performance by spectroscopic analysis, elongating their life span (Figure S33).

Colorful Paper with Efficient Cooling Performance and Esthetics. The compatibility with self-cooling functionality and esthetics requires that a surface reflects a certain wavelength band in the visible region to display colors while maximizing its R_{solar} in near-infrared (NIR) wavelengths (0.7−2.5 μm), where 51% of the solar energy lies to minimize the solar heating, and possessing a high ϵ_{IR} in the atmospheric window (8−13 μm) to radiate heat efficiently to the cold outer space. Red- and green-dyed papers can efficiently reflect the NIR sunlight with a high R_{NIR} of 0.89 and 0.87, respectively, to prevent from being heated up by the NIR solar wavelengths (Figure 9a,b). To further validate the efficient cooling performance of the white and colorful papers under the hot mid-summer weather, mini houses made of the white, yellow, and red-dyed paper composites were fabricated and their "room" temperatures were recorded during the noontime (13:30 to 14:15) on July 9, 2020. The mini houses made of basswood with different colors were selected as control groups (Figures 9c, S34, and S35). We found that the white house made of the cellulose-fiber-based composites was 7.1 °C cooler on average than the ambient air and even 5.3 °C lower on average than that of the basswood-made house (Figure 10a).

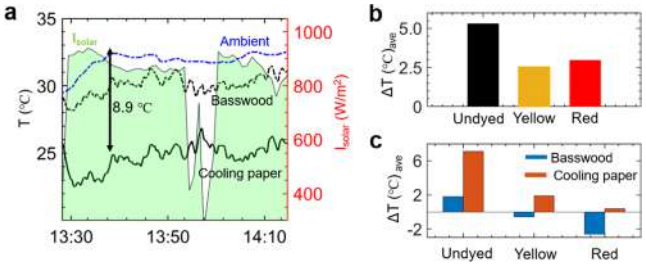

Figure 10. (a) Temperature variations (left axis) and solar intensity (right axis) in the outdoor test of the basswood and paper composites. (b) Average temperature difference of paper composites and the basswood during the test. The temperature of the paper composites is lower than that of the basswood both undyed and yellow/red-dyed. (c) Averaged temperature difference between the ambient and the composites and basswood (undyed, yellow-, and red-dyed). Positive values show that the chamber temperature made of the composites or basswood is lower than the ambient air, and vice versa.

Similar trends of the cooling performance were observed in the yellow and red mini houses made of dyed paper composites and corresponding basswood (Figures 10b,c and S35). The dyed paper composites provide a promising alternative for colored radiative cooling utilization, greatly expanding their scope of applications.

CONCLUSIONS

We demonstrate self-cleaning and self-cooling paper composites made of cellulose-fiber-based paper and PTFE particles that can be scalable-fabricated and easily recycled for PDRC applications. The cellulose-fiber-based composites are super white in the solar wavelengths, resulting from the backscatter of sunlight by the randomized structure of the cellulose microfibers and PTFE microparticles, while it is infrared black in the atmospheric window because of the molecular vibrations of chemical bonds in cellulose and PTFE. The super white and black features at different wavelengths ensure that the paper composites have a net radiative heat loss to the cold outer space. The outdoor experiment demonstrates the excellent cooling effect in both white and colored forms of the composites. Moreover, the paper composites possess a self-cleaning and robust surface, which is a benefit to keeping its good cooling performance for the outdoor environment without labor-intensive maintenance. These multifunctional paper composites provide a promising pathway for practical application in energy-saving and sustainable buildings.

ASSOCIATED CONTENT

Supporting Information

The Supporting Information is available free of charge at https://pubs.acs.org/doi/10.1021/acsami.1c04046.

Reflectivity spectra of the original paper and dust-stained paper, and the composition analysis of the paper composites (Figure S1); SEM images of the original paper and the PTFE particles (Figure S2); contact angle and reflectivity spectra of the paper composites fabricated by different parameters (Figure S3); comparison between the original paper and the paper composites (Figure S4); angle- and polarization-dependent reflectivity spectra of the paper composites (Figure S5); FTIR spectra of the lignin and PTFE (Figure S6); complex refractive indices (Figure S7); light scattering validations of the paper fibers and PTFE particles (Figure S8); reflectivity spectra of the original paper and paper composites and their compositions in different forms (Figure S9); reflectivity comparison of the paper composites and the Black 3.0 painted paper (Figure S10); transmissivity spectra of different layers of paper (Figure S11); setup of the outdoor radiative cooling experiments (Figure S12); temperature tracking, power compensation data analysis and humidity and wind speed over the experimental period (Figure S13); external factors on the radiative paper composites performance (solar intensity and nonradiative heat transfer and atmospheric transmittance) (Figure S14); cooling ability comparison of the paper composites and basswood (Figure S15); humidity and wind speed over the experimental period (Figure S16); optical properties of the paper composites, basswood, and concrete (Figure S17); thermal conductivity comparison of the paper composites, basswood, and concrete (Figure S18); temperature as a function of the net cooling or heating power (Figure S19); mechanical strength tests of the paper composites (Figure S20); self-cleaning tests of the paper composites and water repellence performance of different common materials (Figure S21); photographs of the water contact angles on the paper composites (Figure S22); temperature, humidity, and wind speed over the experimental period (Figure S23); water immersion tests (Figure S24); raindrop tests (Figure S25); abrasion tests (Figure S26); micrograph analysis of the paper composites after abrasion tests (Figure S27); hydrophobic parameter of the paper composites and Photographs showing the water contact angles (Figure S28); spectra analysis after abrasion tests (Figure S29); harsh environment exposure of the paper composites (Figure S30); antiscratch tests and micrographs of the original and paper composites after

https://doi.org/10.1021/acsami.1c04046
ACS Appl. Mater. Interfaces XXXX, XXX, XXX−XXX

scratch tests (Figure S31); tape peel-off tests (Figure S32); spectra analysis of the paper composites after the tape peel-off test and recyclability of the paper composites (Figure S33); average near-infrared and mid-infrared spectral properties and temperature variation of the cooling paper and dyed wood (Figure S34); side view of the setup for the dyed paper composites and dyed basswood outdoor experiment under the clear sky and the humidity, and wind speed over the experimental period (Figure S35); experimental radiative cooling performances reported in other literature (Table S1); physical parameters of the paper composites used in the experiment (Table S2); theoretical model (Supporting Note) (PDF)

One drop of blue-dyed water moves along with the syringe needle, showing the superhydrophobic surface of the self- paper composites (Video S1) (MP4)

AUTHOR INFORMATION

Corresponding Authors

Changyu Tang − *Chengdu Green Energy and Green Manufacturing Technology R&D Center, Chengdu Development Center of Science and Technology, Chengdu 610200, Sichuan, China;* orcid.org/0000-0002-2874-8745; Email: sugarchangyu@163.com

Yi Zheng − *Department of Mechanical and Industrial Engineering, Northeastern University, Boston, Massachusetts 02115, United States; Department of Electrical and Computer Engineering, Northeastern University, Boston, Massachusetts 02115, United States;* orcid.org/0000-0003-4963-9684; Email: y.zheng@northeastern.edu

Authors

Yanpei Tian − *Department of Mechanical and Industrial Engineering, Northeastern University, Boston, Massachusetts 02115, United States*

Hong Shao − *Chengdu Green Energy and Green Manufacturing Technology R&D Center, Chengdu Development Center of Science and Technology, Chengdu 610200, Sichuan, China*

Xiaojie Liu − *Department of Mechanical and Industrial Engineering, Northeastern University, Boston, Massachusetts 02115, United States*

Fangqi Chen − *Department of Mechanical and Industrial Engineering, Northeastern University, Boston, Massachusetts 02115, United States*

Yongsheng Li − *State Key Laboratory Cultivation Base for Nonmetal Composites and Functional Materials, Southwest University of Science and Technology, Mianyang 621010, Sichuan, China*

Complete contact information is available at: https://pubs.acs.org/10.1021/acsami.1c04046

Author Contributions

⊥Y.T. and H.S. contributed equally to this work.

Notes

The authors declare no competing financial interest.

ACKNOWLEDGMENTS

This project is supported by the National Science Foundation through grant number CBET-1941743 and the National Natural Science Foundation of China through grant number 51973245.

REFERENCES

(1) IEA. *The Future of Cooling*. https://www.iea.org/reports/the-future-of-cooling.

(2) Bridgman, P. W. *The Nature of Thermodynamics*; Harvard University Press, 2013.

(3) *Protection, U. S. E. Phaseout of Ozone-Depleting Substances (ODS)*. https://www.epa.gov/ods-phaseout.

(4) Raman, A. P.; Abou Anoma, M.; Zhu, L.; Rephaeli, E.; Fan, S. Passive radiative cooling below ambient air temperature under direct sunlight. *Nature* **2014**, *515*, 540−544.

(5) Zhai, Y.; Ma, Y.; David, S. N.; Zhao, D.; Lou, R.; Tan, G.; Yang, R.; Yin, X. Scalable-manufactured randomized glass-polymer hybrid metamaterial for daytime radiative cooling. *Science* **2017**, *355*, 1062−1066.

(6) Li, T.; Zhai, Y.; He, S.; Gan, W.; Wei, Z.; Heidarinejad, M.; Dalgo, D.; Mi, R.; Zhao, X.; Song, J.; et al. A radiative cooling structural material. *Science* **2019**, *364*, 760−763.

(7) Yang, P.; Chen, C.; Zhang, Z. A dual-layer structure with record-high solar reflectance for daytime radiative cooling. *Solar Energy* **2018**, *169*, 316−324.

(8) Rephaeli, E.; Raman, A.; Fan, S. Ultrabroadband photonic structures to achieve high-performance daytime radiative cooling. *Nano Lett.* **2013**, *13*, 1457−1461.

(9) Chen, Z.; Zhu, L.; Raman, A.; Fan, S. Radiative cooling to deep sub-freezing temperatures through a 24-h day-night cycle. *Nat. Commun.* **2016**, *7*, No. 13729.

(10) Wang, X.; Liu, X.; Li, Z.; Zhang, H.; Yang, Z.; Zhou, H.; Fan, T. Scalable Flexible Hybrid Membranes with Photonic Structures for Daytime Radiative Cooling. *Adv. Funct. Mater.* **2020**, *30*, No. 1907562.

(11) Gentle, A. R.; Smith, G. B. A subambient open roof surface under the Mid-Summer sun. *Adv. Sci.* **2015**, *2*, No. 1500119.

(12) Kou, J.-l.; Jurado, Z.; Chen, Z.; Fan, S.; Minnich, A. J. Daytime radiative cooling using near-black infrared emitters. *ACS Photonics* **2017**, *4*, 626−630.

(13) Zhou, L.; Song, H.; Liang, J.; Singer, M.; Zhou, M.; Stegenburgs, E.; Zhang, N.; Xu, C.; Ng, T.; Yu, Z.; et al. A polydimethylsiloxane-coated metal structure for all-day radiative cooling. *Nat. Sustainability* **2019**, *2*, 718−724.

(14) Chen, Y.; Mandal, J.; Li, W.; Smith-Washington, A.; Tsai, C.-C.; Huang, W.; Shrestha, S.; Yu, N.; Han, R. P.; Cao, A.; Yang, Y. Colored and paintable bilayer coatings with high solar-infrared reflectance for efficient cooling. *Sci. Adv.* **2020**, *6*, No. eaaz5413.

(15) Bhatia, B.; Leroy, A.; Shen, Y.; Zhao, L.; Gianello, M.; Li, D.; Gu, T.; Hu, J.; Soljačić, M.; Wang, E. N. Passive directional sub-ambient daytime radiative cooling. *Nat. Commun.* **2018**, *9*, No. 5001.

(16) Atiganyanun, S.; Plumley, J. B.; Han, S. J.; Hsu, K.; Cytrynbaum, J.; Peng, T. L.; Han, S. M.; Han, S. E. Effective radiative cooling by paint-format microsphere-based photonic random media. *ACS Photonics* **2018**, *5*, 1181−1187.

(17) Zhao, D.; Aili, A.; Zhai, Y.; Lu, J.; Kidd, D.; Tan, G.; Yin, X.; Yang, R. Subambient cooling of water: toward real-world applications of daytime radiative cooling. *Joule* **2019**, *3*, 111−123.

(18) Gentle, A. R.; Smith, G. B. Radiative heat pumping from the earth using surface phonon resonant nanoparticles. *Nano Lett.* **2010**, *10*, 373−379.

(19) Lu, Y.; Sathasivam, S.; Song, J.; Crick, C. R.; Carmalt, C. J.; Parkin, I. P. Robust self-cleaning surfaces that function when exposed to either air or oil. *Science* **2015**, *347*, 1132−1135.

(20) Cai, L.; Peng, Y.; Xu, J.; Zhou, C.; Zhou, C.; Wu, P.; Lin, D.; Fan, S.; Cui, Y. Temperature regulation in colored infrared-transparent polyethylene textiles. *Joule* **2019**, *3*, 1478−1486.

(21) Lozano, L. M.; Hong, S.; Huang, Y.; Zandavi, H.; El Aoud, Y. A.; Tsurimaki, Y.; Zhou, J.; Xu, Y.; Osgood, R. M.; Chen, G.; et al. Optical engineering of polymer materials and composites for

simultaneous color and thermal management. *Opt. Mater. Express* **2019**, *9*, 1990−2005.
(22) Fang, Z.; Zhu, H.; Bao, W.; Preston, C.; Liu, Z.; Dai, J.; Li, Y.; Hu, L. Highly transparent paper with tunable haze for green electronics. *Energy Environ. Sci.* **2014**, *7*, 3313−3319.
(23) Yamada, K.; Shibata, H.; Suzuki, K.; Citterio, D. Toward practical application of paper-based microfluidics for medical diagnostics: state-of-the-art and challenges. *Lab-on-a-Chip* **2017**, *17*, 1206−1249.
(24) Schwanninger, M.; Rodrigues, J.; Pereira, H.; Hinterstoisser, B. Effects of short-time vibratory ball milling on the shape of FT-IR spectra of wood and cellulose. *Vib. Spectrosc.* **2004**, *36*, 23−40.
(25) Tian, Y.; Qian, L.; Liu, X.; Ghanekar, A.; Liu, J.; Thundat, T.; Xiao, G.; Zheng, Y. High-temperature and Abrasion Resistant Metal-insulator-metal Metamaterials. *Mater. Today Energy* **2021**, No. 100725.
(26) Li, Y.; Ren, M.; Lv, P.; Liu, Y.; Shao, H.; Wang, C.; Tang, C.; Zhou, Y.; Shuai, M. A robust and flexible bulk superhydrophobic material from silicone rubber/silica gel prepared by thiol-ene photopolymerization. *J. Mater. Chem. A* **2019**, *7*, 7242−7255.
(27) Abderrahim, B.; Abderrahman, E.; Mohamed, A.; Fatima, T.; Abdesselam, T.; Krim, O. Kinetic thermal degradation of cellulose, polybutylene succinate and a green composite: comparative study. *World J. Environ. Eng* **2015**, *3*, 95−110.
(28) Smith, B. C. *Fundamentals of Fourier Transform Infrared Spectroscopy*; CRC Press, 2011.
(29) Chen, J.; Liu, C.; Wu, S.; Liang, J.; Lei, M. Enhancing the quality of bio-oil from catalytic pyrolysis of kraft black liquor lignin. *RSC Adv.* **2016**, *6*, 107970−107976.
(30) Przybysz, P.; Dubowik, M.; Kucner, M. A.; Przybysz, K.; Przybysz Buzała, K. Contribution of hydrogen bonds to paper strength properties. *PLoS One* **2016**, *11*, No. e0155809.
(31) Mandal, J.; Fu, Y.; Overvig, A. C.; Jia, M.; Sun, K.; Shi, N. N.; Zhou, H.; Xiao, X.; Yu, N.; Yang, Y. Hierarchically porous polymer coatings for highly efficient passive daytime radiative cooling. *Science* **2018**, *362*, 315−319.

https://doi.org/10.1021/acsami.1c04046
ACS Appl. Mater. Interfaces XXXX, XXX, XXX−XXX